SUZAKU BROADBAND OBSERVATIONS OF GALACTIC BLACK HOLE BINARIES: LOW/HARD STATE SPECTRA OF GRO J1655−40

Hiromitsu Takahashi[1], Yasushi Fukazawa[1], Tsunefumi Mizuno[1], Ayumi Hirasawa[1], Shunji Kitamoto[2], Keisuke Sudoh[2], Takayuki Ogita[2], Aya Kubota[3], Kazuo Makishima[4], Motohide Kokubun[4], Takeshi Itoh[4], Arvind N. Parmar[5], Tadayasu Dotani[6], Ken Ebisawa[6], Sachindra Naik[6], Tadayuki Takahashi[6], Kousuke Ohnuki[6], Tahir Yaqoob[7], Lorella Angelini[8], Yoshihiro Ueda[9], Kazutaka Yamaoka[10], Taro Kotani[11], Nobuyuki Kawai[11], Masaaki Namiki[12], Takayoshi Kohmura[13], Hitoshi Negoro[14], and the Suzaku SWG team[15]

[1]*Department of Physical Science, School of Science, Hiroshima University, 1-3-1 Kagamiyama, Higashi-Hiroshima, Hiroshima, 739-8526, Japan*
[2]*Department of Physics, Rikkyo University, 3-34-1, Nishi-Ikebukuro, Toshima–ku, Tokyo, 171-8501, Japan*
[3]*Cosmic Radiation Laboratory, Institute of Physical and Chemical Research (RIKEN), 2-1 Hirosawa, Wako-shi, Saitama, 351-0198, Japan*
[4]*Department of Physics, University of Tokyo, 7-3-1, Hongo, Bunkyo-ku, Tokyo, 113-0033, Japan*
[5]*Astrophysics Mission Division, Research and Scientific Support Department of ESA, ESTEC, Postbus 299, NL-2200 AG Noordwijk, The Netherlands*
[6]*Institute of Space and Astronautical Science, JAXA, 3-1-1, Yoshinodai, Sagamihara, Kanagawa, 229-8510, Japan*
[7]*Department of Physics and Astronomy, John Hopkins University, 3400 N, Charles St., Baltimore, MD 21218, USA*
[8]*Explosion of the Universe Division, NASA Goddard Space Flight Center, Greenbelt, MD 20771, USA*
[9]*Department of Astronomy, Kyoto University, Kitashirakawa-Oiwake-cho, Sakyo-ku, Kyoto, 606-8502, Japan*
[10]*Department of Physics & Mathematics, Aoyama Gakuin University, 5-10-1 Sagamihara, Kanagawa, 229-8558, Japan*
[11]*Department of Physics, Tokyo Institute of Technology, 2-12-1, O–okayama,Meguro-ku, Tokyo, 152-8551, Japan*
[12]*Department of Earth and Space Science, Graduate School of Science, Osaka University, 1-1, Machikaneyama, Toyonaka, Osaka, 560-0043, Japan*
[13]*Physics Department, Kogakuin University, 2665-1, Nakano–cho, Hachioji, Tokyo, 192-0015, Japan*
[14]*Department of Physics, College of Science and Technology, Nihon University, 1-8, Kanda-Surugadai, Chiyoda-ku, Tokyo, 101-8308, Japan*

ABSTRACT

The Galactic black-hole binary GRO J1655−40 was observed with Suzaku on 2005 September 22–23, for a gross time span of ~ 1 day.The source was detected over a wide and continuous energy range of 0.7–300 keV, with an intensity of ∼50 mCrab in the 1.5 – 12 keV band. At an assumed distance of 3.2 kpc, the 0.7–300 keV luminosity is calculated to be $\sim 4.4 \times 10^{36}$ ergs s^{-1}. The source was in a typical low/hard state, since its overall spectrum was dominated by a power-law component with a photon index of ~ 1.7. The source intensity gradually decreased by 20% during the observation, involving little spectral changes above ~ 3 keV. However, at softer energies, the amplitude of variability was somewhat enhanced. This indicates the presence of an independent soft component. The spectra in the hard energy band reveal a high-energy spectral cutoff, with an e-folding energy of ~ 200 keV which is suggested to be higher than those observed from typical black hole binaries in the low/hard state.

Key words: accretion disks — black hole physics — stars: individual (GRO J1655−40)— X-ray: binaries.

1. INTRODUCTION

Suzaku is the fifth Japanese X-ray astronomy satellite launched on 2005 July 10, with an M-V rocket from the Uchinoura space center [34]. It carries 4 sets of X-ray telescopes (XRT, [44]) each with a focal-plane X-ray CCD camera (XIS, X-ray Imaging Spectrometer; [21]) operating in the energy range of 0.2–12 keV, together with a non-imaging Hard X-ray Detector (HXD, [49, 20]), which covers the 10–600 keV energy band. Suzaku has observed four Galactic black-hole binaries (BHBs), GRO J1655−40, Cyg X−1, GRS 1915+105 and 4U 1630−47 [23], in the performance verification phase from 2005 September to 2006 March. The former two were observed in their low/hard state, while the others are in high/soft ones. In this paper, we concentrate on the results of GRO J1655−40. The further detail analysis of this source will be described in the near future [50].

GRO J1655−40 is a transient X-ray source discovered with the BATSE onboard the Compton Gamma Ray Observatory [57]. Subsequent optical observations revealed a 2.6 day binary period [1], and successfully determined the mass of the compact object and mass-donating star as $5.5 - 7.9\ M_\odot$ and $1.7 - 3.3\ M_\odot$, respectively [45]. The

system is thus considered to be a BHB. Together with GRS 1915+105 [33], this object is classified into an interesting subgroup of BHB possessing superluminal radio jets [19]. In addition, GRO J1655−40 allowed the first detection of narrow X-ray absorption lines from ionized iron [51, 54]. The detection of these absorption lines indicates the existence of highly ionized plasmas above the accretion disk. The system inclination of GRO J1655−40 is estimated to be 85° from jet kinematics, or $\sim 70^\circ$ from optical light curves [52]. Although the distance was estimated to be 3.2±0.2 kpc from the radio jet kinematics [19], a shorter distance of less than ~ 1.7 kpc is proposed by [11] based on the spectral type of the secondary star.

Compared to some BHBs that satisfy the standard-disk scenario, e.g. LMC X−3 in particular, GRO J1655−40 exhibits two distinct X-ray peculiarities [30, 24]. One is that its innermost disk temperature $T_{\rm in}$, observed in the high/soft state, is $\sim 40\%$ higher than is predicted by the luminosity and a BH mass of $7M_\odot$. As a result, its innermost disk radius $r_{\rm in}$ turns out to be only 2–3 $R_{\rm g}$, where $R_{\rm g}$ is the gravitational radius. These values are apparently smaller than the radius of the last-stable orbit around a non-spinning BH, 6 $R_{\rm g}$. The other peculiarity is that its excursion from the standard high/soft state into the so-called Very High state [36] starts at a very low luminosity ($\sim$ 0.15 times the Eddington luminosity $L_{\rm E}$), whereas LMC X-3 stays in the standard state up to $\sim L_{\rm E}$. Although these properties are based on an assumed distance of 3.2 kpc, the peculiarities are even more conspicuous if instead the distance of 1.7 kpc [11] is adopted. These unusual properties, together with the radio jets, suggest that GRO J1655−40 harbors a rapidly spinning black hole [59, 30, 24]. We are thus motivated to conduct further high-sensitivity and broad-band X-ray observations of this object.

On 2005 February 17, an X-ray brightening of GRO J1655−40 was detected by the RXTE ASM [31]; since then it remained active for more than half a year. X-ray observations were carried out with XMM-Newton [7, 43], INTEGRAL [7], Swift [3], Chandra [32], and RXTE [46], as the source evolved from the low/hard state into the high/soft state, and then back again. Based on high energy spectra obtained in the low/hard state early in the outburst, [46] reported the detection of high-energy cutoff around 180 keV. In contrast, broad-band spectra taken during the high/soft state reveal a hard tail component extending up to ~ 150 keV [3, 7], reconfirming a previous OSSE detection [22, 58]. The absorption lines from highly ionized ions were also reconfirmed with a blue shift by 300-6000 km s^{-1} [32, 7, 43].

The present paper describes the Suzaku observations of GRO J$1655-40$ made in the decay phase of the 2005 September, while the object was in the low/hard state. We successfully detected the object over an unprecedented wide energy range of 0.7–300 keV. Although the obtained wide-band spectra can be approximated by a power-law of photon index ~ 1.7, the high-quality Suzaku data reveal a spectral cutoff at energies above ~ 100 keV, as well as a weak soft X-ray excess.

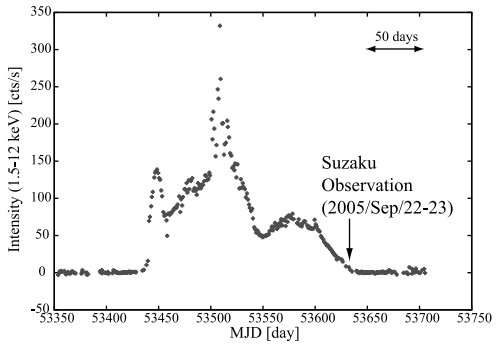

Figure 1. An X-ray (1.5–12 keV) light curve of GRO J1655−40 obtained by the RXTE ASM. The date of the Suzaku observation is indicated by an arrow.

2. OBSERVATION

Using Suzaku, we observed GRO J1655−40 from 2005 September 22, 07:16 UT, through 07:07 UT of the next day. The data were acquired with the XIS and the HXD. As shown in figure 1, the source was at that time in the decay phase of the 2005 outburst, exhibiting a typical 1.5–12 keV intensity of ∼50 mCrab.

The XIS consists of one back-illuminated CCD (BI-CCD) camera and three front-illuminated CCD (FI-CCD) cameras. During the present GRO J1655−40 observation, the XIS was operated in the normal 3×3 and 2×2 mode. Since the source is relatively bright, we employed "1/8 window" option; out of the 1024 rows, 128 rows around the source image are read out. This reduces the frame exposure time to 1 s, and reduces the number of XIS events suffering from pile-up. Furthermore, one of the FI-CCDs (XIS0) was not used in order to double the telemetry capacity of the BI-CCD (XIS1).

The HXD was operated in the normal mode, acquiring 10–70 keV data with the Si PIN photo diodes (hereafter PIN) and 40–600 keV data with the GSO scintillators (hereafter GSO). Combining PIN and GSO with the XIS, Suzaku can cover a wide energy band spanning three orders of magnitude.

The average 0.7–300 keV flux of GRO J1655−40 was measured to be 3.6×10^{-9} erg s^{-1} cm^{-2}. The luminosity in the same band is estimated to be 4.4×10^{36} erg s^{-1} ($\sim 0.006L_{\rm E}$ for a 6 $M_\odot$ black hole), assuming a distance of 3.2 kpc [19].

3. DATA ANALYSIS AND RESULTS

3.1. Data Selection and Background Subtraction

For the XIS data analysis, we extracted cleaned events over good time intervals which were selected by removing spacecraft passages through the South Atlantic

Anomaly (SAA) and periods of low earth elevation ($<$ 20° for the day-time earth and $< 5^\circ$ for the night earth). The details are described in [14]. The source and background events were accumulated in and out of the central $4'.3$ radius of each CCD image, respectively. Although the intensity of GRO 1655−40 was ∼50 mCrab and the "1/8 window" option was employed, we limited the XIS energy range to < 8 keV, in order to avoid possible deformation of the spectral shape due to event pile-up. Since XIS2 and XIS3 have almost the same properties, we hereafter present results obtained from their co-added spectra. The total exposure time is achieved 35 ks per sensor.

Since the HXD does not have offset detectors [49], non X-ray background to be subtracted is synthesized, employing certain models, from the HXD data accumulated during periods of Earth occultation [20]. The models are being developed by the HXD team, and the results are being made publicly available (http://www.astro.isas.jaxa.jp/suzaku/analysis/hxd/hxdnxb/); some early Suzaku publications (e.g., [40, 16]) have actually used the modeled PIN backgrounds. However, GRO J1655−40 was observed only 2 month after the launch, when long-lived activation components in the GSO background spectra were still increasing with a significant rate. Therefore, the model background is thought to be less reliable in this particular case, than in other HXD observations conducted on later occasions. We have hence utilized two types of the background, the modeled background and a blank-sky observation. Since the obtained results with both background subtractions are consistent and the validity of the two methods are confirmed, we hereafter describe only the latter method (see [50] for details).

We derived PIN and GSO background data from an observation of the planetary nebula BD+30°3639, because it was conducted just on the day before (2006 September 21), and no hard X-ray source is catalogued in this sky region. The on-source (i.e., GRO J1655−40) and background (i.e., BD+30°3639) data were both accumulated after removing time periods immediately before (3 minutes) and after (7 minutes) each passage through the SAA, and those when Suzaku was in regions of low geomagnetic cutoff rigidity (< 8 GV). To exclude the periods of Earth occultation, we further screened the on-source data by the condition that the target elevation above the Earth's horizon should be $> 5^\circ$. Then, the background events were accumulated over the same orbital phases of Suzaku as the on-source data integration. The obtained on-source exposure was corrected for dead times, using so-called pseudo events implemented in the HXD [49].As a result, a live time of 20 ks has been attained.

Figure 2 compares the on-source and blank-sky HXD spectra, both obtained in this way. The background-subtracted spectra are also presented. The source is so bright that the signal from GRO J1655−40 exceeds the PIN background even at its upper-bound energy of 70 keV. Therefore, systematic errors of the PIN background are considered to be negligible over the entire PIN energy range (10–70 keV). In the GSO range, the present background can be subtracted with an accuracy of about 2% [50]. As a result, we can claim the source detection with GSO over an energy range of 40–300 keV. Since the GSO background subtraction becomes more subject to systematic errors as the integration time becomes shorter, we hereafter report results from analysis of the GSO data integrated over the entire 20 ks exposure only.

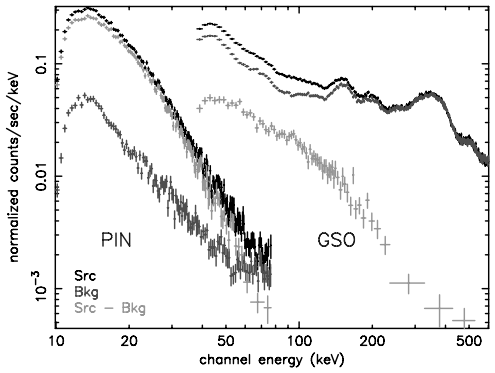

Figure 2. Background subtraction procedure for the HXD data. The on-source data, the background data, and the background-subtracted spectra are presented in black, red, and green, respectively.

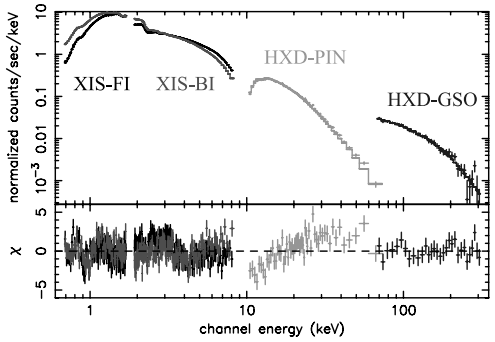

Figure 3. Background-subtracted wide-band (0.7–300 keV) energy spectra of GRO J1655−40, obtained with the XIS, HXD-PIN (green) and HXD-GSO (blue). The spectra of the FI-CCDs (black) and BI-CCD (red) are plotted separately. The bottom panel shows residuals relative to the diskbb+thcomp model fit. In the fitting, the XIS data are utilized in the 0.7–1.7 and 1.9–8 keV ranges, and the GSO data are from the 70–300 keV band.

3.2. Energy Spectra and High Energy Cutoff

Figure 3 shows wide-band energy spectra of GRO J1655−40 from 0.7 keV to 300 keV, obtained with the XIS and HXD, by averaging all the data. In order to assess the overall shapes of these spectra without relying on the detector responses and rather free from possible calibration uncertainties, we first converted them into so-called "Crab ratios", whereby

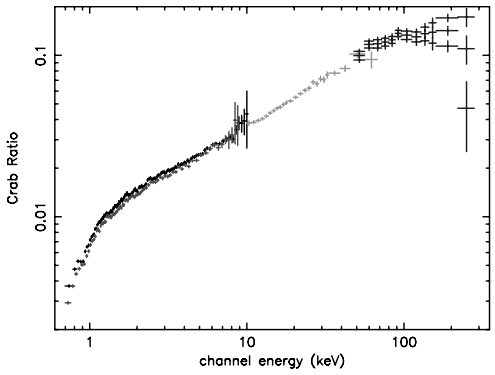

Figure 4. Time-averaged and background-subtracted spectra of GRO J1655−40, divided by the corresponding spectra of the Crab Nebula. GSO data after artificially changing the normalization of the blank-sky background by ±2% are also shown. The colors are the same as in figure 3.

the source spectrum is divided by a Crab spectrum that was accumulated in the same way. As shown in figure 4, the calculated Crab ratio indicates that the object had an intensity of $\sim$ 50 mCrab at 20 keV. The Crab ratio exhibits a nearly constant logarithmic slope of $\sim$ 0.5 in the 2–100 keV range. Considering that the Crab spectrum can be approximated by a power law with a photon index of $\Gamma \sim 2.1$, this implies that the spectrum of GRO J1655−40 also takes a power-law shape, but with $\Gamma \sim 1.6$. We hence conclude that GRO J1655−40 was in the low/hard state during the Suzaku observation. In detail, the slope in the 3–10 keV band is slightly flatter than that in 10–70 keV. The strong drop in the Crab ratio below 1 keV is caused by a higher absorbing column density toward GRO J1655−40 than that to the Crab.

At energies above $\sim$ 100 keV, the Crab ratio in figure 4 exhibits a clear turnover. Since the Crab spectrum, which is about an order of magnitude brighter than that of GRO J1655−40 at $\sim$ 100 keV, is known to exhibit a single power-law shape in the hard X-ray range up to 300 keV or more (e.g., [25]), the hint of turnover in the Crab ratio suggests an intrinsic high-energy cutoff in the GRO J1655−40 spectrum, as is often observed from other BHBs in the low/hard sate. In the figure, the ratios are also plotted by artificially changing the GSO background intensity by ±2%, which is the typical error as described in [50]. Thus, the presence of turnover itself is unaffected by the GSO background uncertainty, although the cutoff steepness varies.

3.3. Light Curves

Figure 5 shows background-subtracted light curves of GRO J1655−40 obtained with the XIS and HXD-PIN. The intensity decreased gradually during this one-day long observation, by $\sim 35\%$ in the softest 0.7–2 keV band and by $\sim 20\%$ in the higher energy bands, resulting in a

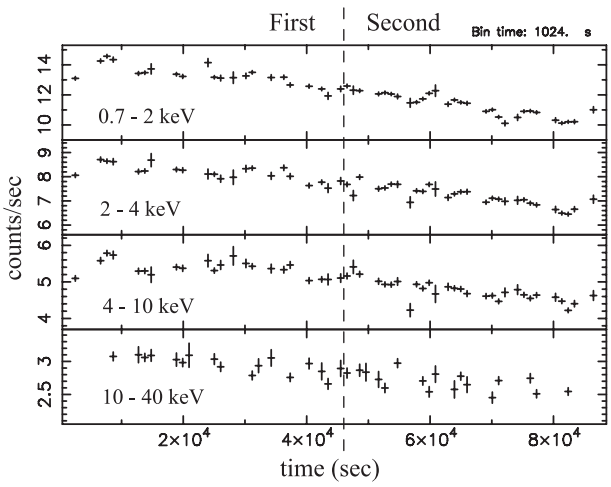

Figure 5. Background-subtracted light curves of GRO J1655−40 obtained with the XIS1 (0.7–2, 2–4, and 4–10 keV) and PIN (10–40 keV). A vertical line divides the exposure into "first" and "second" halves.

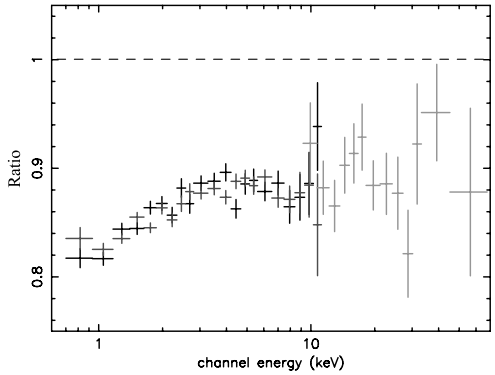

Figure 6. The background-subtracted spectra of GRO J1655−40 obtained with XIS and PIN in the second half, divided by those in the first half.

slight spectral hardening with time. In order to quantify the intensity-correlated spectral changes, we divided the data into two halves, which we hereafter refer to as the first and second halves (figure 5). We then extracted the corresponding energy spectra from the XIS and PIN. The blank-sky PIN background was accumulated over the corresponding portions of the BD+30°3639 observation.

Figure 6 shows spectral ratios between the two halves. The source intensity decreased by $\sim$ 10% above $\sim$ 3 keV, and by up to $\sim$ 18% below $\sim$ 3 keV. Thus, the intensity decrease is somewhat more prominent at low energies, in agreement with the impression from the light curves. (These percentages are smaller than are indicated by the light curves, simply because of time averaging effects.) This suggests the presence of a separate soft spectral component, which is superposed on the dominant power-law shaped continuum emitted over the entire energy band.

3.4. Spectral Model Fittings

3.4.1. The XIS spectra

As a first-cut spectral study, we tried an absorbed single power-law model on the XIS data of GRO J1655−40, as suggested by the Crab ratio in figure 4. Specifically, we fitted the spectrum from the BI-CCD (XIS1) and that from the two FI-CCDs (XIS2 and XIS3 co-added) simultaneously, using the detector responses ae_xi1_20060213c.rmf and ae_xi1_xisnom4_20060415.arf for XIS1, and the average between ae_xi[23]_20060213.rmf and ae_xi[23]_xisnom4_20060415.arf for the co-added FI spectrum. Here and hereafter, fits to the XIS spectra utilize only the 0.7–1.7 keV and 1.9–8 keV ranges, because the excluded energy bands are still subject to calibration uncertainties or possible pile-up effects. The effect of the contamination above the optical blocking filters of the XIS is modeled as additional absorption [21]. In the fitting, we kept the energy offset to be a free parameter within ± 10 eV, which is the current tolerance of the XIS energy scale. The overall model normalization is here and hereafter allowed to differ among different detectors.

The single power-law fit, with a free photon index Γ and a free absorbing column density $N_{\rm H}$ (using the "wabs" model; [37]), was formally rejected by the XIS data with $\chi^2/\nu = 964/416$, mainly due to wiggling residuals at energies below ~ 1.5 keV. This, together with the soft-energy behavior revealed by figure 6, inspired us to incorporate an independent soft component. Evidently, the most natural candidate is an optically-thick disk emission component which is described by the "disk-blackbody (diskbb)" model [35, 29]. We therefore adopted a model consisting of a power-law and a disk blackbody, both absorbed by a common absorber with column density $N_{\rm H}$. This composite model, denoted "diskbb+pow", gave a much improved fit with $\chi^2/\nu = 781/414$, yielding "diskbb" parameters of $kT_{\rm in} \sim 0.26$ keV and an innermost disk radius of $r_{\rm in} = 9/\sqrt{\cos(i)}$ km at a distance of 3.2 kpc, where i is the inclination angle of the disk. Nevertheless, the model was not yet fully acceptable, because of some positive residuals in the 5–7 keV energy range.

Finally we obtained $\chi^2/\nu = 558/411$, by adding a broad ($\sigma = 1.1 \pm 0.1$ keV) Gaussian line component, centered at 6.55 ± 0.10 keV and having an equivalent width of ~ 300 eV. The fit is in fact marginally unacceptable at the 99% confidence level, but is a similar value to those obtained when we fit the Crab spectrum with an absorbed single power-law model. Thus we considered this fitting is essentially acceptable under the current level of instrumental calibration and response adjustments. The obtained best fit parameters are listed in table 1. The power law component has $\Gamma = 1.75$, which is typical of an accreting black hole in the low/hard state. The "diskbb" component has an innermost disk temperature of 0.18 keV, and carries 10.4% of the 0.5–2 keV source flux (or 4.3% in the 0.5–10 keV range). Although the obtained Gaussian parameters are suggestive of a broad iron line or some related spectral feature, we refrain from claiming its reality at present, because we cannot yet rule out the possibility of this feature having an instrumental origin. In subsequent spectral model fittings, we retain this Gaussian in addition to the other model components.

3.4.2. The HXD spectra

Before actually conducting model fittings to the HXD-PIN and GSO spectra of GRO J1655−40, we briefly describe the HXD data of the Crab Nebula. With the current PIN response (ae_hxd_pinxinom_20060814.rsp), the 10–70 keV PIN spectrum of the Crab Nebula can be successfully represented by a single power-law model with $\Gamma = 2.09 \pm 0.01$, which agrees with numerous previous measurements. Similarly, using the GSO response ae_hxd_gsoxinom_20060321.rsp, the 100–300 keV GSO spectrum of the Crab is reproduced to a reasonable accuracy with $\Gamma \sim 2.1$ [20].

Strictly speaking, the single power-law fit to the GSO spectrum of the Crab over the 70–300 keV range, using the current GSO response, is formally unacceptable, due to mild ($\sim 10\%$) convex residuals (see Figure 18 in [20]). This implies that the GSO response predicts slightly too convex spectra than it should. Therefore, the GSO response needs to be improved, or at least corrected, when we try to quantify the high-energy cutoff of GRO J1655−40 suggested by its Crab ratio. In order to make the necessary correction in an explicit manner, we have resorted to introducing an empirical correction factor

$$C(E) \equiv E^{0.65} \exp(-E/230) \ , \qquad (1)$$

where E is the energy in keV, and multiplying this factor to any input model before it is convolved with the current GSO response. This $C(E)$ has a mildly convex shape with a peak at ∼160 keV. In fact, this particular function has been determined so that the current GSO response can successfully reproduce the 70–300 keV spectrum of the Crab Nebula by a single power-law with $\Gamma = 2.1 \pm 0.1$, when the input power-law model is multiplied by $C(E)$. Hereafter in the present paper, we always include this factor $C(E)$ when fitting GSO spectra.

With these preparations, we fitted the HXD (PIN and GSO) spectra of GRO J1655−40, to confirm the high-energy cutoff suggested by figure 4. A single power-law model [but multiplied by equation (1) when simulating the GSO data] failed to give an acceptable joint fit to the PIN and GSO spectra, with $\chi^2/\nu = 167/85$. Since the model was actually over-predicting the GSO data above 100 keV, we replaced the power-law model with a cutoff power-law (hereafter "cutoffpl") model, namely, a power-law multiplied by an exponential factor of the form $\exp(-E/kT_{\rm cut})$, where k is the Boltzmann constant and $T_{\rm cut}$ is the cutoff "temperature". This model has given an acceptable ($\chi^2/\nu = 78/84$) joint fit to the PIN and GSO spectra of GRO J1655−40. The best-fit parameters are listed in table 1, including in particular

Table 1. Best fit parameters of GRO J 1655−40 for the "diskbb+ (pow / cutoffpl / thcomp)" model[*,†]

Data Model	pow / cutoffpl / thcomp $L_{\rm x}$ (erg s^{-1})[‡,§] Photon Index $\cdots$ / $kT_{\rm cut}$ / $kT_{\rm e}$ (keV)	diskbb $L_{\rm x}$ (erg s^{-1})[‡,§] $kT_{\rm in}$ (keV) $r_{\rm in}$ (km)[§,‖]	wabs $N_{\rm H}$[¶]	χ^2/d.o.f
All data (XIS)[#] diskbb+pow	3.93×10^{36} $1.75^{+0.01}_{-0.02}$ $\cdots$	8×10^{34} 0.18 ± 0.01 38^{+7}_{-8}	$7.4^{+0.2}_{-0.3}$	558/411
All data (PIN+GSO) cutoffpl	3.20×10^{36} $1.35^{+0.03}_{-0.04}$ 200 ± 40	$\cdots$ $\cdots$ $\cdots$	$\cdots$ $\cdots$	78/84
All data (XIS+PIN+GSO)[#] diskbb+thcomp	4.43×10^{36} $1.66^{+0.02}_{-0.01}$ > 190	3×10^{34} 0.24 ± 0.01 14^{+5}_{-3}	$6.0^{+0.2}_{-0.1}$	863/496
First half (XIS+PIN)[#] diskbb+thcomp	4.78×10^{36} 1.67 ± 0.01 > 40	5×10^{34} $0.24^{+0.03}_{-0.02}$ 17^{+5}_{-7}	6.0 ± 0.3	633/451
Second half (XIS+PIN)[#] diskbb+thcomp	4.27×10^{36} $1.66^{+0.02}_{-0.01}$ > 40	3×10^{34} $0.22^{+0.03}_{-0.02}$ 15^{+8}_{-6}	6.2 ± 0.3	585/449

[*] Errors refer to 90% confidence limits.
[†] The energy offsets of the XIS spectra are adjusted within < 10 eV.
[‡] The luminosities are in the 0.7–300 keV band.
[§] The distance of 3.2 kpc is assumed.
[¶] In the unit of 10^{21} H atoms cm^{-2}.
[‖] In the unit of $/\sqrt{\cos(i)}$, where i is the inclination of the disk.
[#] A broad Gaussian is added around 6–7 keV. See text in detail.

$\Gamma = 1.35^{+0.03,+0.05}_{-0.04,-0.06}$ and $kT_{\rm cut} = 200^{+40,+200}_{-40,-40}$ keV, where the first errors are statistical and the second ones reflect the 2% systematic uncertainty in the GSO background subtraction.

Through the model fitting to the HXD data, we have thus confirmed quantitatively the presence of the high-energy spectral turnover which is suggested by the Crab ratio. Although the upper bound on $kT_{\rm cut}$ becomes rather loose when considering the GSO systematics, an F-test indicates that the data still prefer the "cutoffpl" model to the single power-law model, because the probability of the cutoff being insignificant is 1×10^{-8}, even if we adopt the worst 2% case of the background estimation. If the correction factor descried by equation (1) is not incorporated, the HXD data of GRO J1655−40 *more strongly* require the high energy cutoff.

3.4.3. Wide-band spectra

Following the above analysis, we next jointly fitted the time-averaged XIS and HXD (PIN and GSO) spectra. Although it would be natural to fit a model consisting of "diskbb" and "cutoffpl" components, here a more physically consistent approach may be adopted. Since the hard X-ray emission from BHBs in the low/hard state is generally interpreted as resulting from thermal Comptonization of some soft photons by hot electrons with a temperature $kT_{\rm e}$ [39],we decided to represent the hard continuum with "thcomp" model by [60], instead of the "cutoffpl" model. We denote this model as "diskbb+thcomp". The "thcomp" model is based on a solution to the Kompaneets equation [28] and successfully describes a thermal cutoff above $E \sim kT_{\rm e}$. In addition, it allows us to use the "diskbb" model itself as a seed photon source: in the fit, we therefore linked the "diskbb" parameters to those of the seed photon distribution in the "thcomp" model. The "thcomp" model has three free parameters: the overall normalization, $kT_{\rm e}$, and the photon index Γ which in turn specifies the Compton optical depth. As before, equation (1) is incorporated in fitting the GSO data.

As shown in table 1 and presented in figure 3, this "diskbb+thcomp" model provided a moderately good joint fit to the three spectra, with $\chi^2/\nu = 863/496$. The photon index turned out to be $\Gamma \sim 1.66$, which is just in between those obtained separately with the XIS (1.75) and the HXD (1.35). The value of $kT_{\rm e}$ is not well constrained because the χ^2 is dominated by contributions associated with the XIS data points, but it is consistent with $kT_{\rm cut}$ derived from the HXD data using the cuoffpl model. The "diskbb" parameters are slightly different from those derived using the XIS data only, because here we expressed the dominant hard continuum by a "thcomp" model instead of a power-law.

*Table 2. Cutoff energy $kT_{\rm cut}$ of other BHBs**

Object	$kT_{\rm cut}$ (keV)	Reference
(Quasi-) persistent sources		
Cyg X−1	150–400	[15, 13, 6, 4]
GRS 1758−258	100–200	[26, 47]
1E 1740.7−2942	~ 50	[48]
Outburst sources		
XTE J1118+480	200–300	[12]
XTE J1550−564	100–300	[2, 42]
GX 339−4	~ 150	[56, 53, 5]
GRO J0422+32	~ 130	[18]
GRS 1716−249	~ 110	[18]
GS 1354−645	~ 90	[41]

* Cutoff energy is assumed 3 times higher than the electron temperature if only the latter is given in the literature.

In addition to the thermal-Comptonization type of continuum, the HXD spectra may well harbor signatures of additional spectral components, including in particular a hump attributable to reflection from an optically-thick accretion disk (e.g., [9, 27]). In fact, the flatter value of Γ indicated by the HXD, than that obtained by the XIS, may be taken as evidence for a reflection component. However, we refrain from performing such detailed analysis, because adding another continuum component would not be justified considering the residual systematic errors in the detector responses.

Finally, we applied the same "diskbb+thcomp" model separately to the first-half and second-half spectra obtained by the XIS and PIN in § 3.3. The results, given in table 1, show that the normalization of the "thcomp" component decreased by $\sim 10\%$, while the photon index stayed constant within the errors. Both the "diskbb" temperature and radius slightly decreased from 0.24 to 0.22 keV and from $17/\sqrt{\cos(i)}$ km to $15/\sqrt{\cos(i)}$ km.As a result, the "diskbb" flux, proportional to $kT_{\rm in}^4\ r_{\rm in}^2$, decreased by $\sim 50\%$. The larger fractional decrease of the flux below 3 keV in figure 6 can be explained as a superposition of the decreases in the "diskbb" temperature and in the intensity of both components.

4. DISCUSSION

We have presented the high-quality broad-band (0.7—300 keV) energy spectra of the black hole candidate GRO J1655−40, obtained with Suzaku in a decay phase of the 2005 outburst when the 0.7–300 keV luminosity was $\sim 4.4\times10^{36}(D/3.2{\rm kpc})^2$ erg s^{-1}. The spectra are characterized by a dominant power law continuum with a photon index of ~ 1.7, a high-energy cutoff, and a weak soft excess. Below, we discuss these characteristics.

4.1. The High Energy Cutoff

Thanks to the high capability of Suzaku, we have shown that the observed high-energy spectrum of GRO J1655−40 gradually deviates, above ~ 100 keV, from a single power-law, and that this "high-energy cutoff" effect can be represented by an exponential factor with $kT_{\rm cut} \sim 200$ keV (or > 100 keV). This reconfirms the INTEGRAL detection of the same feature at a similar energy of ~ 180 keV, made in an early stage of the same outburst [46]; at that time, the object was also in the low/hard state, exhibiting a similar luminosity of $\sim 4\times10^{36}$ erg s^{-1}. These two independent observations firmly establish the presence of a high-energy cutoff in the low/hard state spectrum of GRO J1655−40.

As listed in table 2, the high-energy spectral cutoff has been detected from a fair number of BHBs while they are in the low/hard state. Compared with these measurements, the value of $kT_{\rm cut} = 200^{+40+200}_{-40-40}$ keV we obtained from GRO J1655−40 appears to be higher, although its significance is difficult to quantify. If the possible reflection component is taken into account (§ 3.4.3), we expect the value of $kT_{\rm cut}$ to become even higher.

Assuming that GRO J1655−40 indeed has a rather high cutoff energy, the effect suggests the following two alternative possibilities. One is that the observed luminosity of GRO J1655−40 ($\sim 4\times10^{36}$ erg s^{-1}, or 0.6% Eddington Luminosity for a $6M_\odot$ BH) is somewhat lower than those of the previously observed other sources (typically $\sim 10^{37}$ erg s^{-1}) from which the high-energy cutoff has been detected. In fact, such an anti-correlation between $kT_{\rm cut}$ and the luminosity has been suggested in GRO J0422+32 [10], XTE J1550−564, and some other sources [55]. If so, the decrease of $kT_{\rm cut}$ toward higher luminosities may be attributed to more efficient cooling of the hot electrons by the increased number of soft photons. The other possibility is that the higher value of $kT_{\rm cut}$ is intrinsic to GRO J1655−40, and furthermore, is possibly related to the very high disk temperature of this object in the high/soft state for its mass and luminosity (§ 1; [24]). Though still speculative, it is intriguing to attribute both these properties to a high BH spin.

4.2. The Soft Excess

The XIS spectra require an additional soft-excess component to be added to the power-law continuum (§ 3.4.1). We expressed it in terms of a simple "diskbb" model, and obtained an innermost disk temperature of ~ 0.2 keV together with an innermost disk radius of $r_{\rm in} = 14/\sqrt{\cos(i)} - 38/\sqrt{\cos(i)}$ km, as shown in table 1. Assuming an inclination of $i = 70^\circ$ [52], this yields $r_{\rm in} = 24 - 65$ km, which is equivalent to $1.4 \sim 3.6\ R_{\rm g}$ for a BH of $6M_\odot$ [45]. Thus, the "diskbb" fit implies a cool disk with a rather small radius, which has a bolometric luminosity of $L_{\rm disk} \sim 8\times10^{34}$ erg s^{-1}, or $\sim 1.8\%$ of the observed 0.7–300 keV luminosity (4.43×10^{36} erg s^{-1}). The estimated disk radius is comparable to, or only

a factor of $\sim$2 larger than, those observed from this object in the high/soft state [43, 24].

Although the cool-disk parameters derived above would not in themselves cause immediate problems, it is rather difficult to imagine how a thin cool disk can extend down to a close vicinity of the black hole and is entirely visible to us, whereas 98% of the radiation luminosity is emitted by a separate hot disk, which may fit inside the cool disk or cover its inner portion. This issue may be solved if we consider such conditions as; (1) only a fraction of the accreting mass flow runs through the cool disk, while the rest is bifurcated into the hot disk [8]; (2) only a small fraction of the cool disk is visible to us, while the remaining fraction is occulted (either spatially or temporarily) by the hot disk which must be rather bulging; (3) the inclination may be much higher (e.g. $\sim$85°; [19]).

Although the "diskbb" modeling gives a natural working hypothesis, the soft excess may be explained in alternative ways. For example, it may result from scattering of the continuum by interstellar dust grains. Actually, [17] detected a dust scattering halo around GRO J1655$-$40, and [43] reported changes in the intensity of the scattered component in 24 hours. Yet another possibility is that the soft excess is intrinsic to the hard continuum itself, because the spectrum is known to soften around the peak of "shots" which are responsible for the rapid X-ray variability characteristic of the low/hard state [38]. Then, the observed change in the soft excess intensity could be attributed to variations in the average shot rate.

Through the present analysis, we can confirm the high sensitivity performance of Suzaku. Then, we will resolve the remaining problems in the next step, (1) the existence of the reflection component implied by the difference of the best-fit power-law indices in the XIS and PIN energy ranges, (2) the reality of the broad Gaussian structure around 6.5 keV with an intrinsic width of 1.1 keV, and (3) the variability in the $\sim$ 100 keV energy band on the timescale of $\sim$ ks, which can be studied with the GSO datasets.

REFERENCES

[1] Bailyn, C.D., et al. 1995, Nature, 374, 701

[2] Belloni, T., et al. 2002, A&A, 390, 199

[3] Brocksopp, C., et al. 2006, MNRAS, 365, 1203

[4] Cadolle Bel, M., et al. 2006, A&A, 446, 591

[5] Corongiu, A., et al. 2003, A&A, 408, 347

[6] Di Salvo, T., et al. 2001, ApJ, 547, 1024

[7] Diaz Trigo, M., et al. 2006, A&A, submitted

[8] Done, C., & Kubota, A. 2006, MNRAS 371, 1216

[9] Ebisawa, K., et al. 1996, ApJ, 467, 419

[10] Esin, A.A., et al. 1998, ApJ, 505, 854

[11] Foellmi, C., et al. 2006, astro-ph/0606269

[12] Frontera, F., et al. 2003, ApJ, 592, 1110

[13] Frontera, F., et al. 2001, ApJ, 546, 1027

[14] Fujimoto, R, et al. 2006, PASJ accepted

[15] Gierlinski, M., et al. 1997, MNRAS, 288, 958

[16] Giovanni, M, et al. 2006, PASJ accepted

[17] Greiner, J., et al. 1995, A&A, 297, L67

[18] Grove, J. E., et al. 1998, ApJ, 500, 899

[19] Hjellming R.M. & Rupen M.P. 1995, Nature, 375, 464

[20] Kokubun, M. et al. 2006, PASJ accepted

[21] Koyama, K., et al. 2006, PASJ accepted

[22] Kroeger, R., A., et al. 1996, A&AS, 120, 117

[23] Kubota, A., et al. 2006, PASJ accepted

[24] Kubota, A., et al. 2001, ApJ, 560, L147

[25] Kuiper, L., et al. 2001, A&A, 378, 918

[26] Lin, D., et al. 2000, ApJL, 532, 548

[27] Lightman, A. P., & White T.R. 1988, ApJ, 335, 57

[28] Lightman, A.P., & Zdziarski, A.A. 1987, ApJ, 319, 643

[29] Makishima, K., et al. 1986, ApJ, 308, 635

[30] Makishima, K., et al. 2000, ApJ, 535, 632

[31] Markwardt, C.B., & Swank, J.H. 2005, The Astronomer's Telegram, 414, 1

[32] Miller, J., et al. 2006, Nature, 441, 953

[33] Mirabel, I.F., & Rodriguez, L.F. 1994, Nature, 371,46

[34] Mitsuda, K., et al. 2006a, PASJ accepted

[35] Mitsuda, K, et al. 1984, PASJ, 36, 741

[36] Miyamoto, S, et al. 1991, ApJ, 383, 784

[37] Morrison, R., & McCammon, D. 1983, ApJ, 270. 119

[38] Negoro H., et al. 2001, ApJ, 554, 528

[39] Poutanen, J. & Svensson, R. 1996, ApJ, 470, 249

[40] Reeves, J., et al. 2006, PASJ accepted

[41] Revnivtsev, M. G., et al. 2000, ApJ, 530, 955

[42] Rodriguez, J., et al. 2003, ApJ, 595, 1032

[43] Sala, G., et al. 2006, astro-ph/0606272

[44] Serlemitsos, P. et al., 2006, PASJ accepted

[45] Shahbaz, T., et al. 1999, MNRAS, 306, 89

[46] Shaposhnikov, N., et al. 2006, astro-ph/0609757

[47] Sidoli, L., & Mereghetti, S., 2002, A&A, 388, 293

[48] Sidoli, L., et al. 1999, ApJ, 525, 215

[49] Takahashi, T. et al. 2006, PASJ accepted

[50] Takahashi, H. et al. 2006, PASJ submitted

[51] Ueda, Y., et al. 1998, ApJ, 492, 782

[52] van der Hooft, F., et al. 1998, A&A, 329, 538

[53] Wardzinski, G., et al. 2002, MNRAS, 337, 829

[54] Yamaoka, K., et al. 2001, PASJ, 53, 179

[55] Yamaoka, K., et al. 2005, ChJAAS, 5, 273

[56] Zdziarski, A.A., et al. 1998, MNRAS, 301, 435

[57] Zhang, S.N., et al. 1994, IAU Circl., 6046, 1.

[58] Zhang, S., N., et al. 1997a, ApJ, 479, 381

[59] Zhang, S.N., et al. 1997b, ApJ, 482, L155

[60] Zycki, P., T., et al. 1999, MNRAS, 305, 231